Hindawi
Advances in Polymer Technology
Volume 2022, Article ID 6959485, 12 pages
https://doi.org/10.1155/2022/6959485

Research Article

Vibration Characteristics of Shear Thickening Fluid-Based Sandwich Structures

Ping Wang[1], **Zhiyuan Chen**[1], **Kun Qian**[1,2] **and Kejing Yu**[1]

[1]*College of Textile Science and Engineering, Jiangnan University, Wuxi City, Jiangsu Province, China*
[2]*Key Laboratory of Science & Technology of Eco-Textile, Ministry of Education, Jiangnan University, Wuxi City, Jiangsu Province, China*

Correspondence should be addressed to Kun Qian; qiankun_8@163.com and Kejing Yu; yukejing@jiangnan.edu.cn

Received 30 April 2022; Accepted 9 August 2022; Published 9 September 2022

Academic Editor: Wei Lu

The vibration attenuation mechanism of shear thickening fluid- (STF-) filled sandwich structures was investigated in this study. Structural equivalent damping, stiffness, and mass increased simultaneously with the increase in the volume fraction of shear thickening fluid. However, the damping ratio decreased and natural frequency increased with the increase in structural mass. Thus, the damping ratio was not a monotonically increasing function of the volume fraction of STF. A modified shear strain model of the damping layer was developed based on the following conditions: (1) under the condition of small strain, shear thickening fluid was regarded as linear viscoelastic material, and (2) the warpage of the sandwich beam was considered during deformation and the influence of STF on the shear strain of sandwich beam. According to the modified shear strain model of the damping layer, the shear thickening occurred at 1 Hz to 20 Hz during vibration. Therefore, the resonance point of the structure shifted to the left. The predictions were in excellent agreement with the experimental results. The results demonstrated that shear thickening fluid improved the vibration damping performance of the sandwich structure, while the thickening ability was not the higher, the better.

1. Introduction

Viscoelastic damping sandwich structures have not only high stiffness, light weight, and high deformation resistance but also high damping properties. It is a more widely used damping technology in vibration and noise reduction at present [1]. Although the passive control method has the advantages of low cost and design simplicity, it is difficult to give an effective response to external changes. These weaknesses were resolved by the development of smart materials, such as shape memory polymers (SMPs) [2], magnetorheological (MR) [3], and electrorheological (ER) fluids [4]. Sandwich structures with these smart materials need only an external power supply to be activated and have the advantage of better adaptability to external changes [5]. However, long-term use of external power supply damages other devices due to electric breakdown. One approach to avoiding the requirement of an external power supply is to use a material whose characteristics are changed with the loading conditions [6].

Till 2006, the application of shear thickening fluid (STF) in sandwich structures has grown in importance [7]. STF is composed of particulate phase and carrier fluid, demonstrating a significant increase in viscosity when the shear rate exceeded the critical shear rate. The thickening process is quick and reversible [8]. On account of the remarkable properties, STF is applied to body armors [9, 10], dampers [11], polishing operations [12], and machining processes [13]. After integrating STF with sandwich structures, the stiffness [7] and damping properties [14] of STF-filled sandwich structures can be designed by STF with the different rheological properties. Viscoelastic damping sandwich structures consist of a damping layer (viscoelastic damping materials) and a structural layer [15]. The mismatch of stiffness between the structural layer and damping layer led to large shear deformation of the damping layer and then resulted in increased energy dissipation [16]. Therefore, the dynamic properties of sandwich structures change with the shear rheological property of STF. The shear thickening properties

of STF have been extensively studied [17]. However, there is little research on the impact of the thickening ability of STF on the vibration performance of sandwich structures [18].

Fischer et al. first explored the effect of STF on the dynamic properties of sandwich structures. The results suggested that the resonant frequency and damping raised as the viscosity of STF increased. The stiffness of sandwich structures increased under better interfacial stress transfer [19]. In a separate study published later, the influence of particle morphology on structural dynamic characteristics was investigated. The results reflected that these parameters can directly affect shear moduli of STF, and therefore, the damping properties of the sandwich structure changed [20]. Based on magnetorheological fluid sandwich beam theory, the influence of thickness ratio of the surface layer to the middle layer, excitation frequency, amplitude, and location on the natural frequency of the sandwich structures integrating STF was analyzed by Wei et al. [21]. Gürgen and Sofuoğlu investigated the effects of STF on vibration performance of tubes under different boundary conditions with vibration tests [22]. Later, dynamic properties of PEG-400 and STF-filled sandwich structures were researched for contrast. The experimental results were consistent with Fischer's research conclusions [23]. The starting point for previous studies was strain sensitivity of STF [24, 25]. Additionally, the shear strain of the STF interfacial layer was calculated based on classical beam theory [26]. The effects of STF on the dynamic properties of sandwich structures were deduced by the occurrence of shear thickening behavior. The impact of factors influencing STF rheology, vibration conditions, and structure design on sandwich structures was also considered in other studies. Generally, the vibration attenuation mechanism of shear thickening fluid- (STF-) filled sandwich structures was not deeply studied. The shear strain model of Fischer ignored the warpage of the sandwich beam during deformation and the influence of STF on the shear strain of the sandwich beam [27, 28]. Besides, Newtonian fluids and shear-thinning fluids were neglected in these studies, making it difficult to determine whether the thickening characteristics or the viscous properties of fluid played a role.

In this study, the vibration performance of PEG-400, 18 vol.% STF, 49 vol.% STF, and 61 vol.% STF-filled sandwich structures was studied to demonstrate the vibration attenuation mechanism of STF-filled sandwich structures. The shear rheological measurements were performed to reveal shear rheological behavior. Then, the vibration experiment was conducted to research the influence of PEG and STF on the dynamic properties of sandwich structures. The modified shear strain model was developed to analyze the vibration attenuation mechanism of shear thickening fluid on the vibration performance of sandwich structures.

2. Modeling Shear Strain of Damping Layer

The change in the dynamic properties of sandwich structures was correlated with damping layer rheological response under shear deformation. STF was a shear strain-sensitive material, with its damp and rigid performance increasing when the critical shear strain was exceeded. To analyze the effect of STF on the dynamic properties of sandwich structures, the modified shear strain model based on Fischer's calculation [19] was developed. Previous models ignored the warpage of the sandwich beam during deformation and the influence of STF on the shear strain of the sandwich beam. These conditions were considered when the modified model was established. Shear thickening fluid was regarded as linear viscoelastic material under small strain to simplify the calculation [21].

Figure 1(a) is the schematic diagram of the cantilever sandwich beam filled with STF under external excitation. The sandwich beam consisted of three layers. The lower and upper layers were aluminum alloy with thicknesses of h_1 and h_3, and the middle layer was STF with a thickness of h_2. The length and width of the sandwich beam were a and b, respectively. Based on the classic sandwich plate theory, some assumptions were made about the model. Specifically, (1) the bond of each layer has no slippage during deformation; (2) the transverse displacement w of each layer was equal; (3) the tensile stress along the length direction of the STF layer was ignored; and (4) the section of each layer remained flat after being deformed.

Based on the above assumptions, the x-x section in the STF-filled sandwich beam was taken for analysis. The deformation relationship of the x-x section is illustrated in Figure 1(b) (considering that the STF layer had large shear deformation, the x-x section warped after deformation, and the plane was no longer kept). The displacements of the sections of the lower and upper layers in the x -direction after deformation were u_1 and u_3, respectively; the transverse displacement of each layer in the y -direction was w. Assuming that the displacement of the STF layer in the x -direction was u_2, the shear strain γ of the sandwich beam was expressed as

$$\gamma = \frac{\partial w}{\partial x} + \frac{\partial u_2}{\partial y}, \tag{1}$$

where

$$\frac{\partial u_2}{\partial y} = \frac{u_3 - u_1}{h_2} + \frac{h_3 + h_1}{2h_2}\frac{\partial w}{\partial x}. \tag{2}$$

According to Equation (1), the shear stress was

$$\tau = G^* \cdot \gamma = G^*\left[\left(1 + \frac{h_1 + h_3}{2h_2}\right)\left(\frac{\partial w}{\partial x}\right) + \frac{u_3 - u_1}{h_2}\right], \tag{3}$$

where the complex shear modulus was $G^* = G' + iG''$; G' and G'' denoted the storage modulus and the loss modulus of STF, respectively.

As illustrated in Figure 1(c), the total shear force after the deformation of the x-x section was

$$S = S_1 + S_2 + S_3 = E_1 I_1 \frac{\partial^3 w}{\partial x^3} - \tau h + E_3 I_3 \frac{\partial^3 w}{\partial x^3}, \tag{4}$$

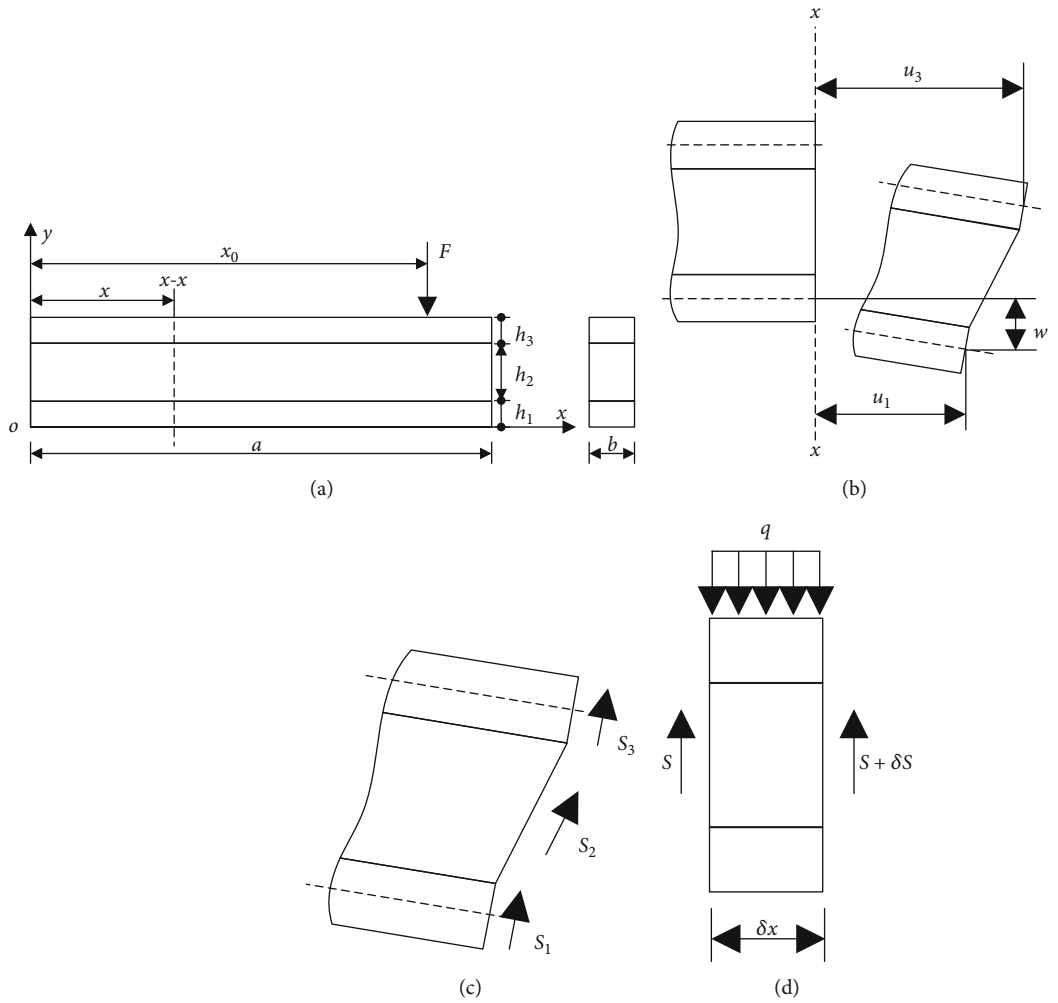

Figure 1: The schematic diagram of (a) cantilever sandwich beam, (b) x-x section, (c) deformed x-x section, and (d) the shear force of the section.

where $h = h_2 + (h_1 + h_3)/2$ and $E_i I_i = E_i h_i^3/12$, $i = 1, 3$; E_1 and E_3 represented the elastic modulus of the lower and upper layers, respectively.

The shear force of the section was related to the transverse distributed load q, obtained from Figure 1(d):

$$S + q\delta x = S + \delta S. \tag{5}$$

From Equation (5), q was the partial derivative of shear force S with respect to x, namely,

$$q = \frac{\partial S}{\partial x}. \tag{6}$$

Given the inertial force of the sandwich beam during deformation, the transverse distributed load q was given as

$$q = -m\frac{\partial^2 w}{\partial x^2} + f(x, t), \tag{7}$$

where m denoted the mass per unit length of the sandwich beam and $f(x, t)$ represented the periodic excitation force, described as

$$f(x, t) = F \exp(i\omega t)\delta(x - x_0), \tag{8}$$

where F and ω indicated the amplitude and frequency of the excitation force, respectively; x_0 denoted the position coordinate of the excitation force; δ represented the Dirac delta function.

Substituting Equations (3) and (4) into Equation (6) yielded

$$q = EI\frac{\partial^4 w}{\partial x^4} - \frac{G^*}{h_2}\left[h^2\frac{\partial^2 w}{\partial x^2} + h\left(\frac{\partial u_3}{\partial x} - \frac{\partial u_1}{\partial x}\right)\right], \tag{9}$$

where $EI = E_1 I_1 + E_3 I_3$.

By taking the partial derivative of γ in Equation (1) with respect to x and substituting the partial derivative into Equation (9) to eliminate u_1 and u_3, it was obtained that

$$\frac{\partial \gamma}{\partial x} = \frac{1}{hG^*}\left(EI\frac{\partial^4 w}{\partial x^4} - q\right). \quad (10)$$

The transverse displacement of the STF-filled sandwich beam in the time domain could be represented as [21]

$$w(x,t) = \sum_{n=1}^{\infty} \sin\left(\frac{n\pi}{a}x\right)\frac{F}{m}\sin\left(\frac{n\pi}{a}x_0\right)\frac{\exp(i\omega t)}{{\omega_n}^2 - \omega^2}, \quad (11)$$

where$\omega_n$represented the$n$ -order natural frequency of the sandwich beam.

Substituting Equations (7), (8), and (11) into Equation (10) yielded

$$\frac{\partial \gamma}{\partial x} = \frac{1}{hG^*}\left[F\exp(i\omega t)\delta(x - x_0) + \sum_{n=1}^{\infty} A\sin \cdot \left(\frac{n\pi}{a}x\right)\sin\left(\frac{n\pi}{a}x_0\right)\frac{\exp(i\omega t)}{{\omega_n}^2 - \omega^2}\right], \quad (12)$$

where

$$A = \frac{F}{m}EI\left(\frac{n\pi}{a}\right)^4 - F\left(\frac{n\pi}{a}\right)^2. \quad (13)$$

The boundary conditions of the cantilever sandwich beam satisfied the following conditions:

(1) The shear strain at the fixed end was 0

$$\gamma(0,t) = 0 \quad (14)$$

(2) The shear rate at the fixed end was 0

$$\frac{\partial \gamma(0,t)}{\partial x} = 0 \quad (15)$$

By integrating Equation (12) through the boundary conditions (14) and (15), the shear strain of the STF layer was obtained as

$$\gamma = \frac{1}{hG^*}\left[xF\exp(i\omega t)\delta(x - x_0) + \sum_{n=1}^{\infty} A\frac{a}{n\pi} \cdot \left(1 - \cos\left(\frac{n\pi}{a}x\right)\right)\sin\left(\frac{n\pi}{a}x_0\right)\frac{\exp(i\omega t)}{{\omega_n}^2 - \omega^2}\right]. \quad (16)$$

3. Materials and Method

3.1. Preparation of STFs and STF-Filled Sandwich Structures. STFs were prepared by dispersing silica particles (from Evonik Degussa Co., Ltd.) with a mean particle size of 650 nm into polyethylene glycol medium with M_w values of 400 (PEG-400, from Sinopharm Chemical Reagent Co., Ltd.). Figure 2(a) exhibits the transmission electron microscope (TEM) images of silica particles. The silica particles were monodisperse and spherical. By obtaining a homogeneous suspension, the sample was placed in a vacuum drying oven for 24 hours at 25°C to remove the bubbles. In the study, STFs at the conditions of different concentrations (18 vol.%, 49 vol.%, and 61 vol.% for SiO_2) were produced.

STF-filled sandwich structures were prepared by one layer of 3 mm thick STF and two layers of 1 mm thick aluminum alloy (5052 type aluminum alloy). Silicone rubber with a width and a thickness of 3 mm was applied for sealing around the sandwich beams. A bakelite with a length of 30 mm, a width of 10 mm, and a thickness of 3 mm was placed at the clamping end. Figure 2(b) displays STF-filled sandwich structures, with the dimension of $260 \times 10 \times 5\,mm^3$.

3.2. Method

3.2.1. Rheology Tests. The rheological behavior of PEG and STF was explored by an Anton-Paar Physica MCR 301 rheometer. The steady-shear experiments were performed with 25 mm diameter parallel plates. The frequency sweep and strain amplitude sweep tests were conducted on a cone plate with a diameter of 50 mm and an angle of 1°.

3.2.2. Vibration Tests. The vibration experiment was conducted by the vibration beam testing (VBT) set-up to investigate the influence of PEG and STF on the dynamic properties of sandwich structures, as illustrated in Figure 3. The boundary conditions of all samples were single-fixed. One end of the sample was clamped, and the other end was excited to generate vibration from a shaker (MS-100). The force signal was collected by a piezoelectric pressure sensor (CL-YD-303). The sandwich beam acceleration signal was measured by the acceleration sensor (KISTLER 8640A50). The power spectrum of the vibration signal was obtained by CRAS modal analysis software. The experimental design is presented in Table 1. The neat sandwich structure is sealed with silicone rubber to ignore the effect of silicone rubber on the damping.

4. Results and Discussion

4.1. Rheological Behavior

4.1.1. Steady-State Rheological. The steady-state shear rheological curve of PEG-400, 18 vol.% STF, 49vol.% STF, and 61 vol.% STF is illustrated in Figure 4. PEG-400 was the dispersion medium of shear thickening fluid. As a Newtonian fluid, the viscosity of PEG-400 did not change with the shear rate. With the addition of silica particles, rheological properties and initial viscosity of PEG-400 solution presented various kinds. Terminal hydroxyl and abundant oxygen atoms in PEG-400 formed a considerable number of hydrogen bonds with the silanol groups of silica particles [29]. Hence, the initial viscosity of STF was greater than that of PEG-400. 18 vol.% STF presented as non-Newtonian shear-thinning fluids. In the initial stages, electrostatic force and Brownian force acted on silica particles. The particles

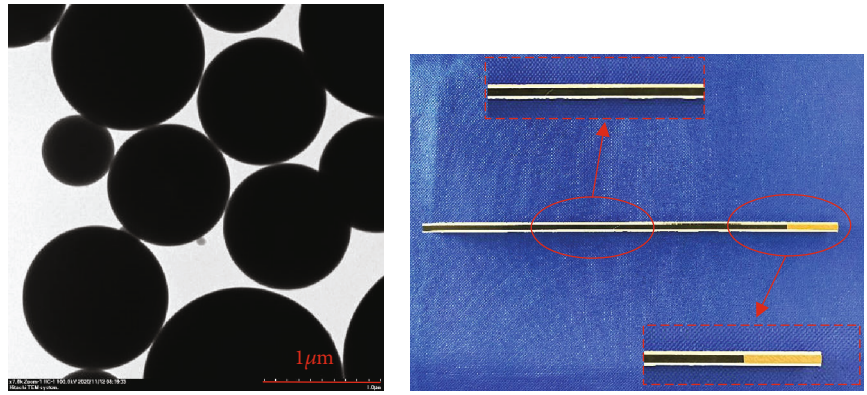

Figure 2: (a) TEM image of silica particles. (b) Image of sandwich structures.

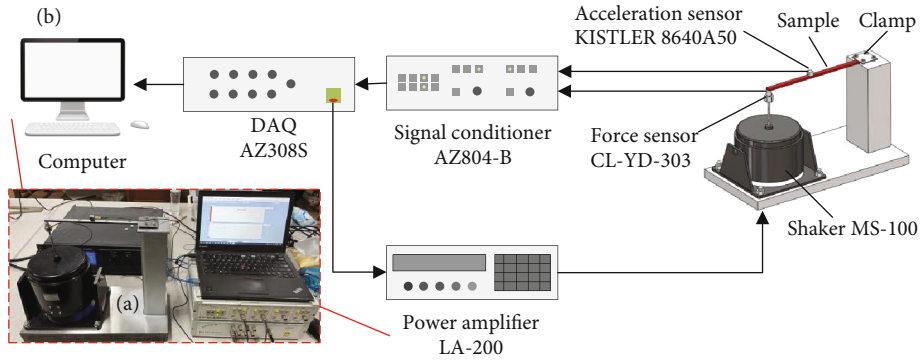

Figure 3: (a) Image of vibration test and (b) the schematic diagram of VBT set-up.

Table 1: The experimental design of vibration tests.

Specimen code	Specimen design	Average weight (g)
NSS	Net sandwich structure	20.39
SSF-PEG	Sandwich structure filled with PEG-400	24.83
SSF-STF18	Sandwich structure filled with 18 vol.% STF	25.48
SSF-STF49	Sandwich structure filled with 49 vol.% STF	26.30
SSF-STF61	Sandwich structure filled with 61 vol.% STF	27.25

repelled one another and were arranged orderly. With the increasing shear rate, the original aggregates of particles were dispersed. According to the hydrodynamic cluster theory [30], the collisions between particles were neglected when the number of silica particles was small. Therefore, 18 vol.% STF possessed shear-thinning property. Besides, 49 vol.% STF exhibited continuous shear thickening (CST) behavior, and its viscosity slowly increased at the thickening stage. Additionally, 61 vol.% STF had a discontinuous shear thickening (DST) phenomenon, and its viscosity increased rapidly at the transition point. Chen et al. [31] investigated microstructural features of STF. The force between silica particles changed from hydrodynamic forces to contact friction force, resulting in the transition from CST to DST. A stable friction contact network was formed along with the DST phenomenon occurring. The silica particles were subject to compression during the DST stage [25, 32].

4.1.2. Dynamic Rheological. The changes in structure's damping and stiffness were induced by the STF's dynamic viscoelastic characteristics [33]. Considering that the frequency and strain varied in vibration, the effects of frequency and strain amplitude on the viscoelasticity of the damping layer were explored. The viscoelastic moduli of PEG-400 and STF versus angular frequency at the strain of 100% are presented in Figure 5(a). The storage and loss modulus of PEG-400 and 18 vol.% STF increased linearly in the range of 0.1-100 rad/s. The viscoelasticity analysis of STF was inconsistent with previous steady-state rheological analysis. This was an artifact due to low torque. PEG-400

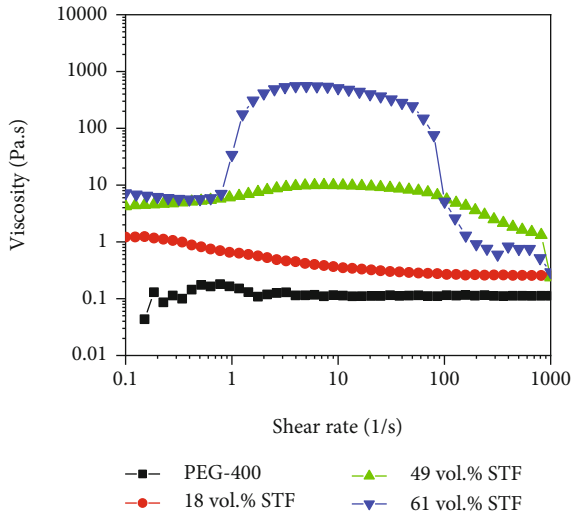

FIGURE 4: The steady-state shear rheological curve of PEG-400, 18 vol.% STF, 49 vol.% STF, and 61 vol.% STF.

mainly exhibited elasticity characteristics because its storage modulus was higher than the loss modulus. After the addition of silica particles, the viscous properties of mixtures were significant since the particle chain breakage resulted in permanent deformation when the angular frequency was high. The modulus of 61 vol.% STF changed suddenly in which significant nonlinear viscoelastic behavior appeared.

Regarding most polymer solutions, the strain amplitude in the linear region was generally 0.01–0.1. The nonlinear region appeared with the increase in the strain [34]. The large amplitude oscillatory shear (LAOS) tests were performed to characterize the nonlinear viscoelastic properties of STF. Figure 5(b) exhibits the LAOS tests of PEG-400 and STF at the angular frequency of 1.5 rad/s. The variation of modulus was consistent with the frequency sweep tests. Figures 5(c)–5(d) illustrate dynamic rheological tests carried out on 49 vol.% STF and 61 vol.% STF to analyze the effect of strain and angular frequency on shear thickening behavior. These results implied that shear thickening occurred more easily with the increase in the strain and angular frequency. Fourier rheology was a general quantitative method for LAOS tests. In the linear region, the stress response contained none but the first harmonic, while the multiharmonic response was observed in the nonlinear region [35, 36]. The output moduli measured by the method of LAOS tests generally were the first-harmonic moduli. Figures 5(a)–5(d) suggest that it was difficult to characterize the nonlinear properties of materials because the contribution of higher order was ignored. G_L', G_M', η_L', and η_M' were defined to study the instantaneous nonlinear characteristics. The local tangent modulus at $\gamma = 0$ of the elastic Lissajous-Bowditch curves was G_M' (minimum-strain modulus), and local secant modulus at $\gamma/\gamma_0 = x = 1$ of the elastic Lissajous-Bowditch curves was G_L' (large-strain modulus) [37]; similarly, η_M' and η_L' represented the modulus at the lowest and highest shear rates, respectively. According to the graphics demonstration, the parameters of quantitative nonlinear characteristics were also defined. The strain-stiffening ratio (S) and the shear thickening ratio (T) can be obtained by

$$S = \frac{G_L' - G_M'}{G_L'} = \frac{4e_3 + \cdots}{e_1 + e_3 + \cdots}, \tag{17}$$

$$T = \frac{\eta_L' - \eta_M'}{\eta_L'} = \frac{4v_3 + \cdots}{v_1 + v_3 + \cdots}, \tag{18}$$

where $S = 0$ demonstrated linear response, $S > 0$ suggested strain stiffening with one cycle, and $S < 0$ indicated strain softening with one cycle. $T = 0$ represented linear response, $T > 0$ signified shear thickening with one cycle, and $T < 0$ amounted to shear thinning with one cycle. The minimum-strain modulus G_M' equated to the zero-strain elasticity, whereas the large-strain modulus G_L' captured the large strain elasticity. Furthermore, the strain-stiffening ratio S correctly captured the true relative magnitude of the intracycle strain stiffening. A similar approach defined shear thickening ratio T. η_M' captured the viscous material coefficient at zero shear rate, whereas η_L' represented the viscous material coefficient at maximum strain rate. The sign of S and T was determined by e_3 and v_3, respectively. The degree of nonlinear contribution was measured by e_3/e_1 and v_3/v_1. Among them, e_3 and v_3 were dominant components in nonlinear response, and e_1 and v_1 were linear components. Therefore, the changes of e_3/e_1 and v_3/v_1 values should be analyzed at different frequencies and strains [34].

The measured e_3/e_1 and v_3/v_1 values from LAOS tests of 49 vol.% STF and 61 vol.% STF with the angular frequency at 1.5 rad/s are presented in Figures 6(a) and 6(b). The results revealed that the elastic nonlinearity of 61 vol.% STF was strain softening ($e_3 < 0$) under a small strain; after that, the strain hardening appeared ($e_3 > 0$). Additionally, 49 vol.% STF first exhibited elastic linearity ($e_3 = 0$). Gradually, the elastic properties changed from linearity to strain hardening. With the increase in STF concentration, the e_3/e_1 values were added. The reason was that the more the silica particles of STF, the longer the length of particle chains. At the oscillatory shear strain, more particle chains twisted and rotated. Thus, the performance of elasticity of 61 vol.% STF became better. As reflected in Figure 6(b), the viscous nonlinearity of 49 vol.% STF and 61 vol.% STF improved little by little with the increasing strain. The variation trend of the ratio of viscous coefficients was similar to the elastic coefficients' ratios. More particle chains increased resistance to particle motion. Therefore, the viscous properties of 61 vol.% STF were enhanced. Comparative analysis implied that the e_3/e_1 values increased and the viscous deformation occurred at small strains with the increase of the volume fraction of STF. Figures 6(c)–6(f) illustrate 49 vol.% STF and 61 vol.% STF elastic and viscous coefficients' ratios in the angular frequency range from 0.15 to 1.5 rad/s. These data indicated that the e_3/e_1 values and v_3/v_1 values rose as the angular frequency increased. Under dynamic conditions, the critical point $\gamma_m\omega$ of STF was a fixed value. Before reaching the

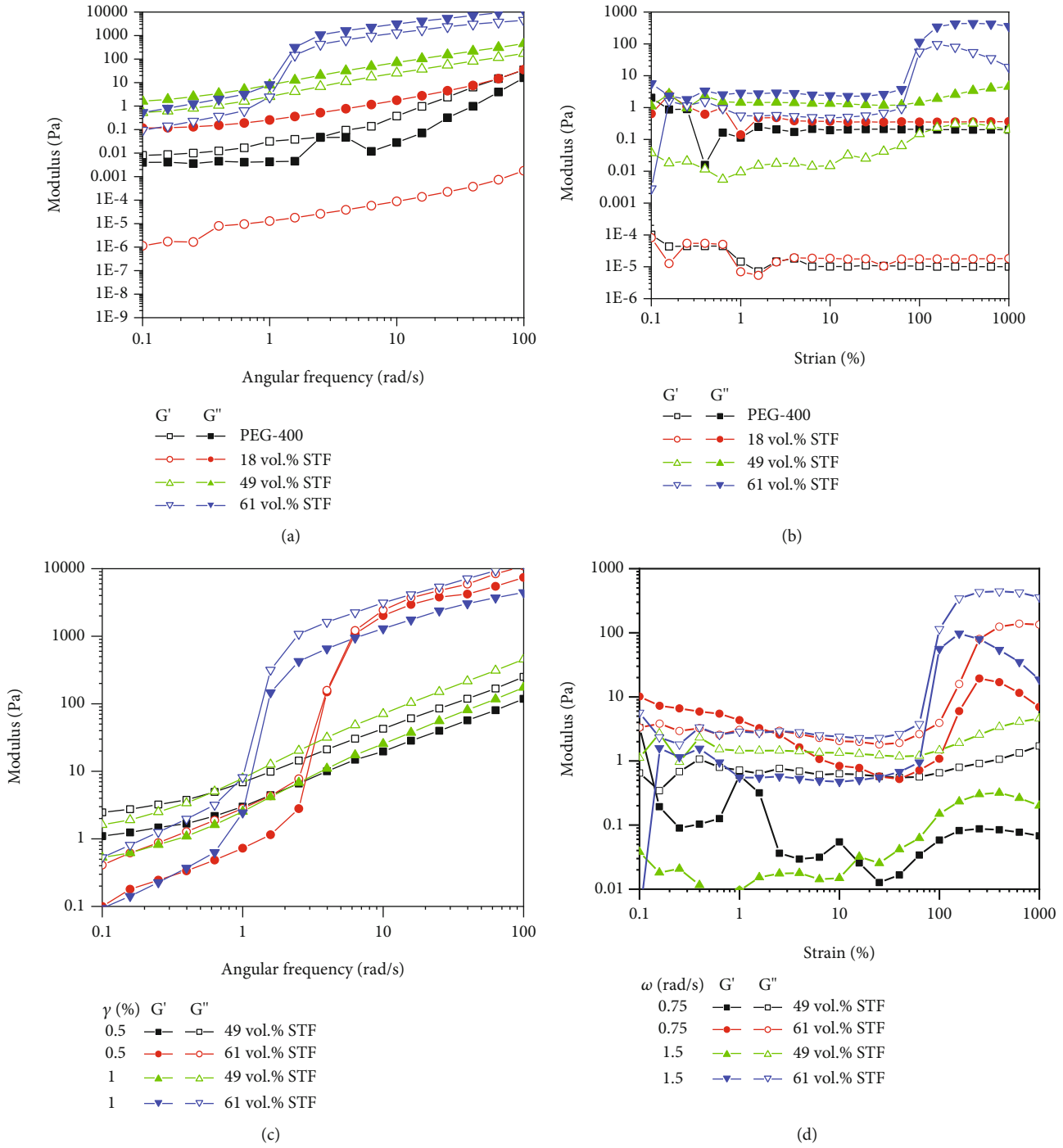

Figure 5: (a) Frequency sweep at the strain of 100% and (b) LAOS test with the angular frequency at 1.5 rad/s for PEG-400 and STF. (c) Frequency sweep in the strain range from 0.5 and 1 and (d) LAOS test in the angular frequency range from 0.75 to 1.5 rad/s of 49 vol.% STF and 61 vol.% STF.

critical point, the greater the angular frequency, the higher the viscoelastic moduli. Thus, elastic and viscous coefficients ratios increased [38].

4.2. Dynamic Response of the Sandwich Structure. Figure 7(a) provides a frequency response curve of NSS. The frequency corresponding to the peak value of vibration acceleration was the natural frequency ω_n. According to the half-power bandwidth method [39], the damping ratio ζ was calculated by

$$\zeta = \frac{f_2 - f_1}{2\omega_n}, \tag{19}$$

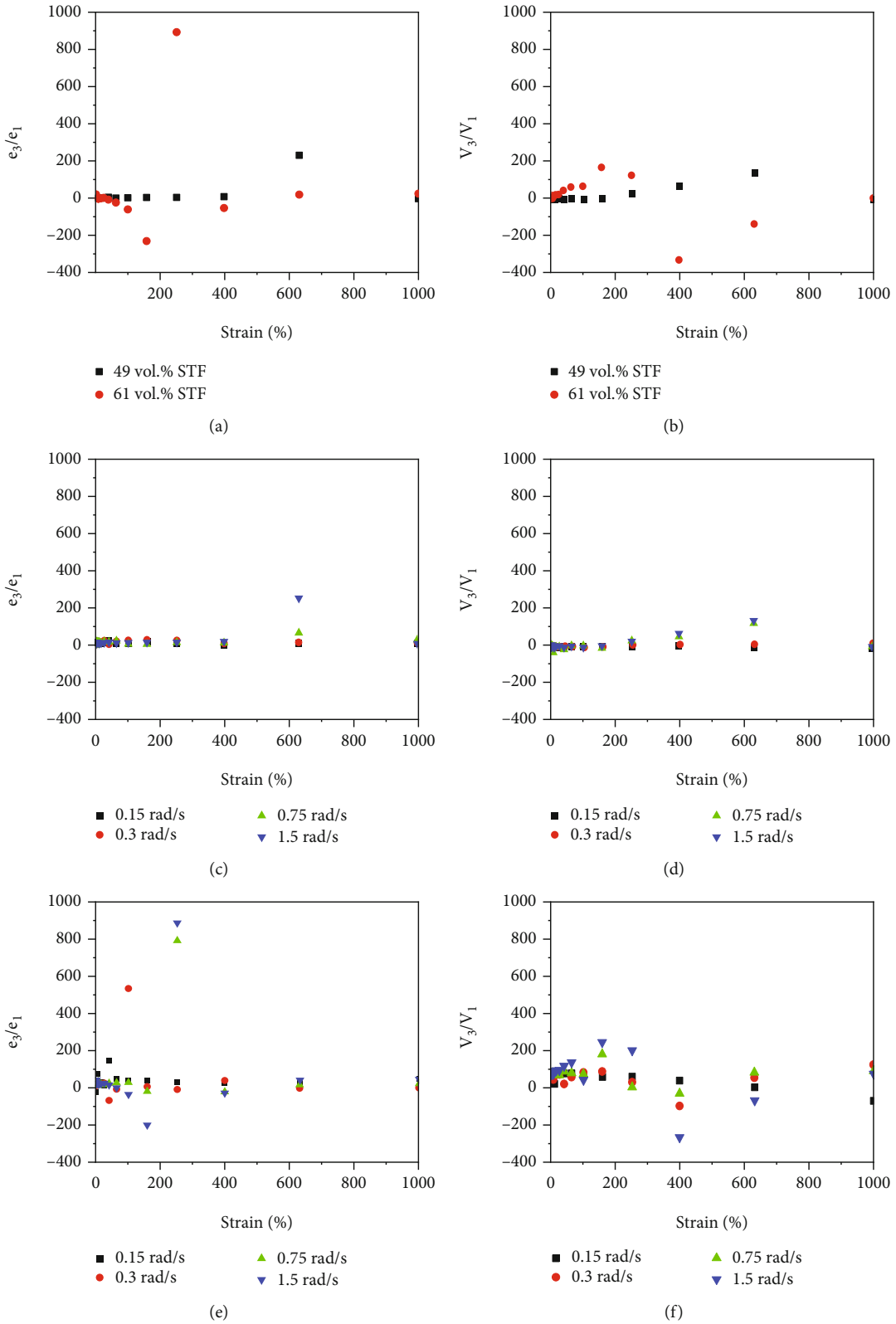

FIGURE 6: (a) The e_3/e_1 values and (b) the v_3/v_1 values of 49 vol.% STF and 61 vol.% STF with the angular frequency at 1.5 rad/s. (c) The e_3/e_1 values and (d) the v_3/v_1 values of 49 vol.% STF in the angular frequency range from 0.15 to 1.5 rad/s. (e) The e_3/e_1 values and (f) the v_3/v_1 values of 61 vol.% STF in the angular frequency range from 0.15 to 1.5 rad/s.

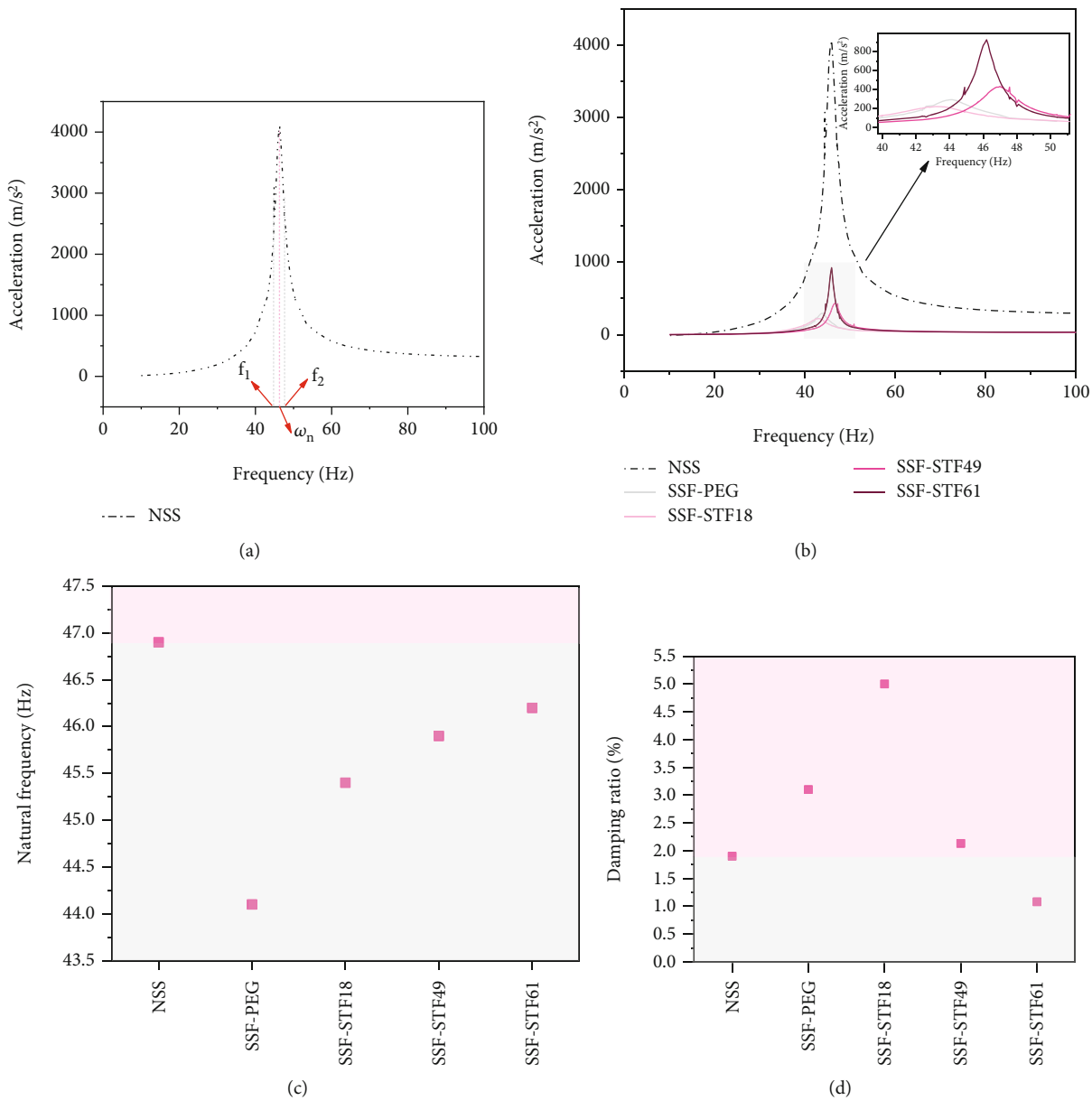

FIGURE 7: The frequency response curve of (a) NSS and (b) NSS, SSF-PEG, SSF-STF18, SSF-STF49, and SSF-STF61. (c) The natural frequency and (d) damping ratio of each specimen.

where f_1 and f_2 denoted the frequency corresponding to 0.707 time peak value. Owing to different damping layers, the natural frequency and damping ratios of the structure were changed in variety, as presented in Figure 7(b).

The natural frequencies of each specimen are illustrated in Figure 7(c). With the increasing content of silica particles, the natural frequency increased and became lower than that of the neat sandwich structure. The natural frequency of the sandwich structure was affected by the mass matrix and stiffness matrix. Bending stiffness was related to the moment of inertia and elastic modulus. It can be obtained that

$$D = EI_Z, \tag{20}$$

where E and I_Z represented elastic modulus and moment of inertia, respectively. The moment of inertia of rectangular section was

$$I_Z = \frac{BH^3}{12}, \tag{21}$$

where B and H denoted the width and height of the rectangular, respectively. Generally, the moment of inertia of the rectangular hollow section was smaller than that of the rectangular solid section. According to Equation (21), the moment of inertia of the hollow section was that of a solid section of the same width and height minus that of a solid section, which was the same size as the middle hollow

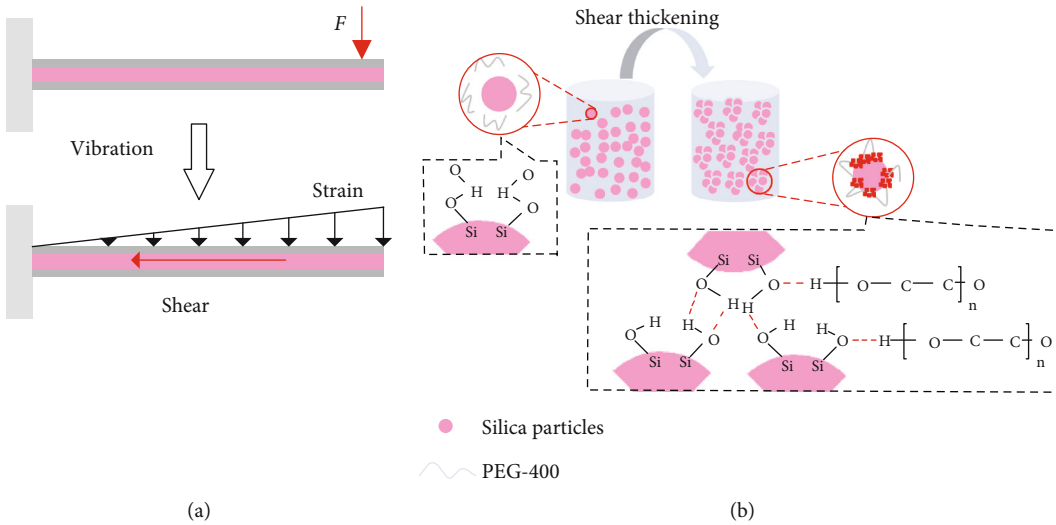

FIGURE 8: (a) The stress and strain distributions of STF-filled sandwich structures during vibration. (b) The thickening mechanism of STF.

section [40]. Thus, the moment of inertia of the neat sandwich structure was the smallest. The elastic moduli of the lower and upper aluminum alloy layers were 70 GPa. However, the maximum modulus of elasticity in shear of the viscous liquid was about 10^5 Pa. The farther away from the neutral layer, the larger the normal stress was. Under the same stress, the strain of the neat sandwich structure was slightly lower than that of the viscous fluid-filled sandwich structure. Therefore, the bending stiffness of the neat sandwich structure was a little higher. The viscoelastic moduli of mixtures were enhanced with the increase in silica particles' volume fraction. Moreover, the natural frequency rose when the modulus was improved. The variation trend of the natural frequency with damping layers was consistent with these inferences. The influence of stiffness on natural frequency was stronger than that of mass in these samples. Consequently, the effect of mass on natural frequency was not discussed in this part.

Figure 7(d) exhibits the damping ratio of each sandwich structure. The damping ratio rose first and then decreased with increasing silica particles. The damping ratio could be computed as

$$\zeta = \frac{c_{eq}}{2\sqrt{k_{eq}m}}, \tag{22}$$

where c_{eq} and k_{eq} denoted equivalent damping and equivalent stiffness, respectively. The damping ratio of sandwich structure was proportional to equivalent damping and inversely proportional to equivalent stiffness and mass of sandwich structure. The equivalent damping was decided by the viscous properties of STF; the equivalent stiffness was determined by the elastic moduli of the lower and upper aluminum and STF. Obviously, with the increasing of volume fraction of SiO_2, equivalent damping, equivalent stiffness, and mass of sandwich structure increased. When the volume fraction of SiO_2 was 18%, the increase in equivalent damping played a major role. With the further increase of volume fraction of SiO_2, the increase in equivalent stiffness and mass determined the damping ratio. Therefore, at higher silica loadings, damping got lower.

The constrained damping layer was mainly subjected to shear during vibration. The dynamic properties of sandwich structures were primarily connected with the shear properties of the damping layer [41]. PEG-400 belonged to Newtonian fluid, and its viscosity did not vary with the shear strain. Nonetheless, the damping properties of STF were distinct under different shear strain conditions. The action of the damping layer on structural dynamic performance was analyzed by the previous shear strain model. In this study, x was set to be a, and the maximum strain was obtained by simplifying Equation (16):

$$\gamma_{max} = \frac{aF\cos(\omega t)}{hG^*}. \tag{23}$$

The vibration test results suggested that the exciting force of each sample was about 10^{-2} N. The values of a and h were constant, and the $\cos(\omega t)$ values were from 0 to 1. The maximum strain was affected by the complex shear modulus alone. The γ_{max} of 61 vol.% STF and 49 vol.% STF was estimated to be 10^{-3}% and 1%, respectively, following the Cox-Merz rule [42]:

$$\eta(\dot{\gamma}) = \eta^*(\gamma_m \omega). \tag{24}$$

The shear thickening occurred at 1–20 Hz under dynamic conditions. Therefore, the resonance point of the structure shifted to the left after adding STF. The vibration attenuation mechanism of STF-filled sandwich structures is illustrated in Figure 8. Equation (16) indicated that the shear strain of STF was different. As demonstrated by Figure 8(a), the shear strain depended on where STF was. The shear thickening behavior occurred when the shear strain was greater than the critical shear strain, as indicated in Figure 8(b). PEG 400 formed ether hydrogen bonds in multiple positions on the surface of silica particles, or hydrogen

bonds might be formed between one end group hydroxyl and surface silanol group. Hydrogen bonds may also be formed between PEG-400 molecules and silica particles. Compared with the one end group hydroxyl, the silanol groups were more acidic. PEG-400 was more likely to bond with silica particles than to form hydrogen bonds between PEG-400 molecules [43]. The formation of particle chain increased E and c_{eq}. Additionally, the natural frequency of the neat sandwich structure was larger than that of the viscous fluid-filled sandwich structure since the maximum E value was smaller than 70 GPa. ζ was proportional to c_{eq}. Nevertheless, k_{eq} and m remarkably affected the structural damping ratio. Therefore, ζ was not a monotonically increasing function of silica particles.

5. Conclusions

The vibration characteristics of fluids with different rheological properties filled with sandwich structures were investigated in this study. The results did not demonstrate that the larger the thickening ability, the better the vibration damping performance of the sandwich structure. STF improved the stiffness and damping properties of sandwich structures as a result of its high viscosity. With the increasing content of silica particles, the natural frequency and equivalent damping of STF-filled sandwich structures increased. According to the modified shear strain model of the damping layer, shear thickening behavior occurred under fixed strain amplitudes. Besides, the energy dissipation and stress transfer increased owing to the shear thickening effect. However, STF significantly influenced the mass of the structure, which increased by 33.6% in max. With the increasing mass, the damping ratio decreased, and natural frequency increased. Therefore, the vibrational properties were not monotonically increasing functions of the content of STF. The results demonstrated that after integrating STF with sandwich structures, sandwich structures filled with STF give effective response on external changes without external power supply. Sandwich structures filled with STF can be used for aeronautics, transportation, and buildings. In all these applications, adaptive control of structural vibration is realized by shear rate sensitivity of STF.

Data Availability

The data used to support the findings of this study are available from the corresponding authors upon request.

Conflicts of Interest

There are no conflicts to declare.

Acknowledgments

This work was supported by the Postgraduate Research & Practice Innovation Program of Jiangsu Province (KYCX20_1786) and the Fundamental Research Funds for the Central Universities (JUSRP51907A, JUSRP51718A).

References

[1] M. S. H. Al-Furjan, Y. Yang, A. Farrokhian, X. Shen, R. Kolahchi, and D. K. Rajak, "Dynamic instability of nano-compositepiezoelectric-leptadenia pyrotechnica rheological elastomer-porous functionally graded materials micro visco-elastic beams at various strain gradient higher-order theories," *Polymer Composites*, vol. 43, no. 1, pp. 282–298, 2022.

[2] P. Butaud, E. Foltête, and M. Ouisse, "Sandwich structures with tunable damping properties: on the use of shape memory polymer as viscoelastic core," *Composite Structures*, vol. 153, pp. 401–408, 2016.

[3] P. Yang, M. Yu, J. Fu, S. Liu, S. Qi, and M. Zhu, "The damping behavior of magnetorheological gel based on polyurethane matrix," *Polymer Composites*, vol. 38, no. 7, pp. 1248–1258, 2017.

[4] K. Esteki, A. Bagchi, and R. Sedaghati, "Dynamic analysis of electro- and magneto-rheological fluid dampers using duct flow models," *Smart Materials and Structures*, vol. 23, no. 3, article 035016, 2014.

[5] M. Karimiasl and H. Ahmadi, "Theoretical investigation on the buckling behavior of smart composite sandwich panels with viscoelastic core and shape memory alloy included skins," *Polymer Composites*, vol. 42, no. 10, pp. 5361–5373, 2021.

[6] S. Gürgen and M. A. Sofuoğlu, "Smart polymer integrated cork composites for enhanced vibration damping properties," *Composite Structures*, vol. 258, article 113200, 2021.

[7] J. Yang, S. Sun, N. Guo et al., "Development of a smart rubber joint for train using shear thickening fluids," *Smart Materials and Structures*, vol. 29, no. 5, article 055036, 2020.

[8] J. Warren, S. Offenberger, H. Toghiani, C. U. J. Pittman, T. E. Lacy, and S. Kundu, "Effect of temperature on the shear-thickening behavior of fumed silica suspensions," *ACS Applied Materials and Interfaces*, vol. 7, no. 33, pp. 18650–18661, 2015.

[9] J. Ge, Z. Tan, W. Li, and H. Zhang, "The rheological properties of shear thickening fluid reinforced with SiC nanowires," *Results in Physics*, vol. 7, pp. 3369–3372, 2017.

[10] M. R. Sheikhi and S. Gürgen, "Anti-impact design of multi-layer composites enhanced by shear thickening fluid," *Composite Structures*, vol. 279, article 114797, 2022.

[11] Z. Lu, Z. Wang, Y. Zhou, and X. Lu, "Nonlinear dissipative devices in structural vibration control: a review," *Journal of Sound and Vibration*, vol. 423, no. 1, pp. 18–49, 2018.

[12] S. Gürgen and A. Sert, "Polishing operation of a steel bar in a shear thickening fluid medium," *Composites Part B: Engineering*, vol. 175, article 107127, 2019.

[13] S. Gürgen and M. A. Sofuoğlu, "Integration of shear thickening fluid into cutting tools for improved turning operations," *Journal of Manufacturing Processes*, vol. 56, pp. 1146–1154, 2020.

[14] K. Lin, A. Zhou, H. Liu, Y. Liu, and C. Huang, "Shear thickening fluid damper and its application to vibration mitigation of stay cable," *Structure*, vol. 26, pp. 214–223, 2020.

[15] C. Zhang and K. T. Tan, "Low-velocity impact response and compression after impact behavior of tubular composite sandwich structures," *Composite Part B: Engineering*, vol. 193, article 108026, 2020.

[16] F. D. S. Eloy, G. F. Gomes, A. C. Ancelotti, S. S. D. Cunha, A. J. F. Bombard, and D. M. Junqueira, "A numerical-experimental dynamic analysis of composite sandwich beam with magnetorheological elastomer honeycomb core," *Composite Structures*, vol. 209, pp. 242–257, 2019.

[17] K. Fu, H. Wang, Y. X. Zhang et al., "Rheological and energy absorption characteristics of a concentrated shear thickening fluid at various temperatures," *International Journal of Impact Engineering*, vol. 139, article 103525, 2020.

[18] S. Cao, Q. Chen, Y. Wang, S. Xuan, W. Jiang, and X. Gong, "High strain-rate dynamic mechanical properties of Kevlar fabrics impregnated with shear thickening fluid," *Composites Part A: Applied Science and Manufacturing*, vol. 100, pp. 161–169, 2017.

[19] C. Fischer, S. A. Braun, P. E. Bourban, V. Michaud, C. J. G. Plummer, and J. A. E. Månson, "Dynamic properties of sandwich structures with integrated shear-thickening fluids," *Smart Materials and Structures*, vol. 15, no. 5, pp. 1467–1475, 2006.

[20] C. Fischer, A. Bennani, V. Michaud, E. Jacquelin, and J. A. E. Månson, "Structural damping of model sandwich structures using tailored shear thickening fluid compositions," *Smart Materials and Structures*, vol. 19, no. 3, article 035017, 2010.

[21] M. Wei, G. Hu, L. Jin, K. Lin, and D. Zou, "Forced vibration of a shear thickening fluid sandwich beam," *Smart Materials and Structures*, vol. 25, no. 5, article 055041, 2016.

[22] S. Gürgen and M. A. Sofuoğlu, "Experimental investigation on vibration characteristics of shear thickening fluid filled CFRP tubes," *Composite Structures*, vol. 226, article 111236, 2019.

[23] S. Gürgen and M. A. Sofuoğlu, "Vibration attenuation of sandwich structures filled with shear thickening fluids," *Composite Part B: Engineering*, vol. 186, article 107831, 2020.

[24] K. Fu, H. Wang, L. Chang, M. Foley, K. Friedrich, and L. Ye, "Low-velocity impact behaviour of a shear thickening fluid (STF) and STF-filled sandwich composite panels," *Composites Science and Technology*, vol. 165, pp. 74–83, 2018.

[25] K. Chen, Y. Wang, S. Xuan, and X. Gong, "A hybrid molecular dynamics study on the non-Newtonian rheological behaviors of shear thickening fluid," *Journal of Colloid and Interface Science*, vol. 497, pp. 378–384, 2017.

[26] J. Y. Yeh, "Vibration analysis of sandwich rectangular plates with magnetorheological elastomer damping treatment," *Smart Materials and Structures*, vol. 22, no. 3, article 035010, 2013.

[27] V. Birman and G. A. Kardomateas, "Review of current trends in research and applications of sandwich structures," *Composite Part B: Engineering*, vol. 142, pp. 221–240, 2018.

[28] Q. Sun, J. X. Zhou, and L. Zhang, "An adaptive beam model and dynamic characteristics of magnetorheological materials," *Journal of Sound and Vibration*, vol. 261, no. 3, pp. 465–481, 2003.

[29] W. Yang, Y. Wu, X. Pei, F. Zhou, and Q. Xue, "Contribution of surface chemistry to the shear thickening of silica nanoparticle suspensions," *Langmuir*, vol. 33, no. 4, pp. 1037–1042, 2017.

[30] H. Nakamura, S. Makino, and M. Ishii, "Continuous shear thickening and discontinuous shear thickening of concentrated monodispersed silica slurry," *Advanced Powder Technology*, vol. 31, no. 4, pp. 1659–1664, 2020.

[31] K. Chen, Y. Wang, S. Xuan, S. Cao, and X. Gong, "Contribution of frictional contact during steady and oscillatory shear in the discontinuous shear thickening fluid," *Smart Materials and Structures*, vol. 28, no. 4, article 045009, 2019.

[32] D. Xu, J. L. Hawk, D. M. Loveless, S. L. Jeon, and S. L. Craig, "Mechanism of shear thickening in reversibly cross-linked supramolecular polymer networks," *Macromolecules*, vol. 43, no. 7, pp. 3556–3565, 2010.

[33] R. C. Neagu, P. E. Bourban, and J. A. E. Månson, "Micromechanics and damping properties of composites integrating shear thickening fluids," *Composites Science and Technology*, vol. 69, no. 3-4, pp. 515–522, 2009.

[34] D. Coblas, D. Broboana, and C. Balan, "Correlation between large amplitude oscillatory shear (LAOS) and steady shear of soft solids at the onset of the fluid rheological behavior," *Polymer*, vol. 104, pp. 215–226, 2016.

[35] K. Hyun, M. Wilhelm, C. O. Klein et al., "A review of nonlinear oscillatory shear tests: analysis and application of large amplitude oscillatory shear (LAOS)," *Progress in Polymer Science*, vol. 36, no. 12, pp. 1697–1753, 2011.

[36] T. B. Goudoulas, S. Pan, and N. Germann, "Nonlinearities and shear banding instability of polyacrylamide solutions under large amplitude oscillatory shear," *Journal of Rheology*, vol. 61, no. 5, pp. 1061–1083, 2017.

[37] R. H. Ewoldt, A. E. Hosoi, and G. H. McKinley, "New measures for characterizing nonlinear viscoelasticity in large amplitude oscillatory shear," *Journal of Rheology*, vol. 52, no. 6, pp. 1427–1458, 2008.

[38] M. Kamkar, S. Sadeghi, M. Arjmand, and U. Sundararaj, "Structural characterization of CVD custom-synthesized carbon nanotube/polymer nanocomposites in large-amplitude oscillatory shear (LAOS) mode: effect of dispersion characteristics in confined geometries," *Macromolecules*, vol. 52, no. 4, pp. 1489–1504, 2019.

[39] G. V. Narayana and N. Ganesan, "Critical comparison of viscoelastic damping and electrorheological fluid core damping in composite sandwich skew plates," *Composite Structures*, vol. 80, no. 2, pp. 221–233, 2007.

[40] T. C. Lim, *Auxetic Materials and Structures*, Springer, Singapore, 2015.

[41] R. Manoharan, R. Vasudevan, and A. K. Jeevanantham, "Dynamic characterization of a laminated composite magnetorheological fluid sandwich plate," *Smart Materials and Structures*, vol. 23, no. 2, article 025022, 2014.

[42] Y. S. Lee and N. J. Wagner, "Dynamic properties of shear thickening colloidal suspensions," *Rheologica Acta*, vol. 42, no. 3, pp. 199–208, 2003.

[43] W. Jiang, F. Ye, Q. He et al., "Study of the particles' structure dependent rheological behavior for polymer nanospheres based shear thickening fluid," *Journal of Colloid and Interface Science*, vol. 413, pp. 8–16, 2014.